



Efficacy of delayed ^{18}F -FDG hybrid PET/MRI for epileptic focus identification: a prospective cohort study

Fang Liu^{1,2} · Weiwei Ruan^{1,2} · Xuejun Deng³ · Yangmeihui Song^{1,2} · Wenyu Song^{1,2} · Fan Hu^{1,2} · Jinxia Guo⁴ · Xiaoli Lan^{1,2}

Received: 21 January 2020 / Accepted: 17 June 2020 / Published online: 25 June 2020
© Springer-Verlag GmbH Germany, part of Springer Nature 2020

Abstract

Objective We sought to investigate the contribution of delayed ^{18}F -FDG imaging data to epileptogenic zone (EZ) identification using a hybrid positron emission tomography/magnetic resonance imaging (PET/MRI) system.

Methods Forty-one patients with epilepsy underwent a brain dual time point ^{18}F -FDG PET/MRI examination. All early imaging was acquired at approximately 40 min. Late imaging was classified as short delay (150.1 ± 20.2 min) or long delay (247.8 ± 24.6 min). Visual evaluation and scoring of ^{18}F -FDG uptake at dual time points were performed. An SUV_{mean} asymmetry index (AI) was calculated representing the difference in uptake between the EZ and the contralateral side. The EZ location was defined by a multidisciplinary team based on findings on video electroencephalography, ^{18}F -FDG, and MRI. EZ location was classified as extratemporal lobe epilepsy (extra-TLE) or temporal lobe epilepsy (TLE). MRI findings were classified as positive if there were signal/structural abnormalities, or negative. AI of dual time points was compared between MRI-positive and MRI-negative, between extra-TLE and TLE, and between short delay and long delay of the late imaging time point.

Results The AI at the delayed time points was increased by a mean of 3.7 over the early time point in all patients ($P < 0.01$). The biggest AIs were found in the MRI-positive group. The ΔAI between two imaging points were 3.71 ± 3.50 and 4.67 ± 7.94 for MRI-positive and MRI-negative; 4.52 ± 6.70 and 2.51 ± 2.42 for extra-TLE and TLE; and 4.24 ± 6.52 and 3.46 ± 2.90 for short delay and long delay groups, respectively. There were more patients with increased AI at the delayed time with MRI-positive (95.8%, 23/24), with extra-TLE (96.8%, 30/31), and with short delay time (93.7%, 30/32). Two observers who had no knowledge of the images chose 85.4% and 82.9% of the delay-time point images as the more obvious asymmetry from all images. The kappa value between the two observers was 0.66 with good agreement.

Conclusion Delayed ^{18}F -FDG PET imaging can be used to better identify EZs with relatively greater metabolic asymmetry between the EZ and contralateral regions.

Keywords Epilepsy · ^{18}F -FDG · Hybrid PET/MRI · Delayed imaging · Asymmetry index

This article is part of the Topical Collection on Neurology

✉ Xiaoli Lan
xiaoli_lan@hust.edu.cn; lxl730724@hotmail.com

¹ Department of Nuclear Medicine, Union Hospital, Tongji Medical College, Huazhong University of Science and Technology, No. 1277 Jiefang Ave, Wuhan 430022, China

² Hubei Province Key Laboratory of Molecular Imaging, Wuhan 430022, China

³ Department of Neurology, Union Hospital, Tongji Medical College, Huazhong University of Science and Technology, Wuhan, China

⁴ GE Healthcare, Shanghai 201203, China

Introduction

Epilepsy is a clinical syndrome characterized by abnormal excessive, synchronous neuronal activity in the brain, occurring in 0.5–1% of the overall population [1]. Detection of the epileptogenic zone (EZ) responsible for seizure onset can improve seizure control and is necessary in presurgical evaluation. The EZ is usually associated with brain structural abnormalities, such as those resulting from trauma, intracranial tumors, intracranial inflammation, genetic/metabolic diseases, and developmental abnormalities. Structural abnormalities can be shown on computed tomography (CT) or magnetic resonance imaging (MRI) [2]; however, the EZ does not always correspond with a given structural abnormality, and 20–

30% of patients with epilepsy have normal high-resolution MRI examinations [3, 4].

At present, an effective and accurate modality to localize EZs remains a major challenge. Besides electroencephalography (EEG) and MRI, ^{18}F -FDG PET imaging, which demonstrates metabolic activity, plays an important role in detecting EZs, especially for those with negative MRI findings [5, 6]. PET has a sensitivity of 70–90% in temporal lobe epilepsy (TLE) and 33–67% in extratemporal TLE (extra-TLE) for localization of EZs [7]. PET affects surgical strategy in 50–70% of cases, and 17% of cases rely on PET imaging alone to determine surgical decisions [3].

Dual time point imaging (DTPI) in ^{18}F -FDG PET is a technique in which imaging data are acquired at an early time point of 45–60 min after ^{18}F -FDG injection and at a delay time point, which can range from minutes to hours. DTPI PET is often used in the detection of glioma, brain tumor classification, and distinction of tumor recurrence from radiation necrosis [8–11]. It is generally agreed that delayed imaging could provide more informative than early imaging to distinguish malignant from benign lesions [12, 13]. To the best of the authors' knowledge, there has been no study focused on DTPI in the evaluation of EZs. The aim of this study was to evaluate the efficacy of delayed time point ^{18}F -FDG PET/MRI for the identification of EZs using several quantitative criteria.

Patients and methods

Patients and groups

This prospective study was permitted by the Research Ethics Committee of the Huazhong University of Science and Technology. All adult patients and the parents of pediatric patients gave written informed consent prior to enrollment in this study.

From 24 May 2018 to 28 Sep. 2018, a total of 41 patients, including 26 males and 15 females, age from 13 to 69 years (mean 29.6 ± 14.4 years), were included in this study (Table 1). The inclusion criteria for patients were (1) a history of epilepsy > 2 years and (2) available diagnostic data including detailed neurologic history, physical examination, interictal and/or ictal scalp video electroencephalogram (VEEG), and routine MRI. Exclusion criteria included (1) < 12 years of age; (2) hyperglycemia or severe metabolic disease; (3) brain tumor; and (4) contraindications for MRI examination.

Based on MRI, the patients were divided into the MRI-positive group (abnormal structure and/or signal on MRI, $n = 24$, including 7 cases of encephalomalacia with gliosis, 5 cases of hippocampal sclerosis, 3 cases of arachnoid cyst compressing the adjacent parenchyma, 3 cases of

polymicrogyria, 3 cases of chronic hemorrhagic foci, 2 cases of focal cortical dysplasia, and 1 case of gray matter heterotopia) and the MRI-negative group (no structural or signal abnormalities on MRI, $n = 17$).

The locations of EZs were determined by a multidisciplinary team (MDT) consisting of an epileptologist (with 25 years of clinical experience) and two neuroradiologists (with 20 years of MRI experience and 15 years of PET experience) according to clinical history, VEEG results, ^{18}F -FDG PET/MRI, 3D arterial spin labeling perfusion-weighted imaging (3D ASL-PWI), and routine MRI. For each examination, the weight of the importance for EZ localization is in order of VEEG (epileptiform discharge): localization > lateralization > uncertain; MR (structure/intensity abnormality): MR positive > MR negative; ^{18}F -FDG (hypometabolism on either early or delayed ^{18}F -FDG): focal > multiple; 3D ASL-PWI (hypoperfusion): consistent with FDG > uncertain. For all the examinations, the weight of the importance for EZ localization is in order of VEEG > ^{18}F -FDG PET > MRI. 3D ASL-PWI is the supplement to ^{18}F -FDG, which can increase the diagnosis confidence. The EZ localization can be determined when at least two of the three examinations (VEEG, MRI, either early or delayed ^{18}F -FDG + 3D ASL-PWI) were consistent in localization (Table 2). Depending on the MDT diagnosis, patients were described as extratemporal lobe epilepsy (extra-TLE, $n = 31$) or temporal lobe epilepsy (TLE, $n = 10$).

Based on the delayed imaging interval, the patients' image acquisitions were described as short delay with imaging time of 150.1 ± 20.2 min ($n = 32$) after injection of ^{18}F -FDG or long delay with imaging time of 247.8 ± 24.6 min ($n = 9$), respectively.

PET/MRI protocol

All the patients were interictal during PET/MRI examination. The PET/MRI examinations were within 3–120 days (mean, 12.1 days) from the last seizure. The patients fasted for at least 6 h before the PET/MRI examination and the blood glucose level was confirmed to be < 140 mg/dL. ^{18}F -FDG 3.7 MBq/kg (0.1 mCi/kg) was intravenously injected. After resting calmly for about 40 min, the patients underwent the first brain PET/MRI examination, and then returned to the waiting room for rest before the acquisition of the delayed images. The delayed images were acquired 2.5–4 h later according to the clinical arrangement.

PET/MRI acquisition

The brain imaging was performed with a hybrid time-of-flight (TOF) PET/MRI (SIGNA™ PET/MRI, GE Healthcare, Waukesha, WI, USA). Both PET acquisitions were performed in 3D mode with 15 min/bed position (DFOV = 30 cm). The PET datasets were reconstructed with a 192×192 matrix (pixel size, $1.5625 \times 1.5625 \times 2.78$ mm³) with TOF and point

Table 1 Demographic and clinical data of all 41 patients

Patient no.	Gender	Age (years)	VEEG localization	FDG localization	MRI findings and localization	EZ localization by MDT	Late imaging
1	M	22	R/F	R/F	R/F/EM	R/F	Short delay
2	M	55	L/Lat	L/O	L/O/EM	L/O	Short delay
3	F	31	R/O	R/O	R/O/EM	R/O	Short delay
4	F	24	L/Lat	L/P-O	L/P/EM	L/P	Short delay
5	M	14	L/F	L/F	L/F/EM	L/F	Short delay
6	M	69	R/Lat	R/F-P	R/P/EM	R/P	Short delay
7	M	29	R/Lat	R/F-T	R/F/EM	R/F	Short delay
8	M	18	R/T	R/T	R/T/HS	R/T	Short delay
9	F	55	L/T	L/T	L/T/HS	L/T	Short delay
10	F	27	Uncertain	L/T	L/T/HS	L/T	Short delay
11	M	28	L/T	L/T	L/T/HS	L/T	Short delay
12	M	18	Uncertain	L/T	L/T/HS	L/T	Short delay
13	M	27	R/F-P	R/P	R/T/AC	R/P	Long delay
14	M	13	R/Lat	R/F	R/F/AC	R/F	Short delay
15	M	15	L/Lat	L/F	L/T/AC	L/F	Long delay
16	F	16	R/Lat	R/F-P	R/F/PMG	R/F	Long delay
17	F	30	R/O	R/O	R/O/PMG	R/O	Short delay
18	M	29	R/F	R/Lat	R/F-P/PMG	R/F	Short delay
19	F	67	L/P	L/P	L/P/HF	L/P	Long delay
20	M	61	R/F	R/F	R/F/HF	R/F	Short delay
21	M	33	R/F	R/F	R/F/HF	R/F	Short delay
22	F	21	R/P	R/P	R/F/FCD	R/P	Short delay
23	F	20	L/P	L/P	L/P/FCD	L/P	Short delay
24	F	27	Uncertain	R/O	R/O/HTP	R/O	Short delay
25	M	42	L/T	L/T	Negative	L/T	Short delay
26	M	32	R/T	R/F-T	Negative	R/T	Short delay
27	M	31	L/F	L/F	Negative	L/F	Short delay
28	F	27	R/Lat	R/F-T	Negative	R/F	Short delay
29	M	17	R/Lat	R/P-O	Negative	R/O	Long delay
30	F	50	L/Lat	L/F	Negative	L/F	Short delay
31	M	19	R/Lat	R/F	Negative	R/F	Long delay
32	M	40	L/F-T	L/F	Negative	L/F	Short delay
33	F	27	L/P	L/P	Negative	L/P	Short delay
34	M	19	L/Lat	L/I	Negative	L/I	Long delay
35	M	18	L/T	L/T	Negative	L/T	Short delay
36	F	39	L/F-T	L/F	Negative	L/F	Short delay
37	F	15	R/Lat	R/F	Negative	R/F	Short delay
38	M	16	L/Lat	L/T	Negative	L/T	Short delay
39	M	21	L/F	L/F	Negative	L/F	Short delay
40	M	22	L/F-T	L/T	Negative	L/T	Long delay
41	M	30	L/Lat	L/P	Negative	L/P	Long delay

R right, L left, F frontal, I insula, O occipital, P parietal, T temporal, Lat lateralization, MDT multidisciplinary team, EM encephalomalacia, HS hippocampal sclerosis, AC arachnoid cyst, PMG polymicrogyria, HF hemorrhagic foci, FCD focal cortical dysplasia, HTP heterotopia

spread function (PSF) ordered subset expectation maximization (OSEM) algorithms with 28 subsets and 3 iterations, followed by a 3-mm Gaussian filter. The MRI sequences were

simultaneously started with PET acquisition at the same bed position. MR attenuation correction (MRAC) used the atlas-based method.

Table 2 Neuroimaging results of all 41 patients

Neuroimaging technique	Localization	Lateralization	Uncertain/negative
VEEG	23	15	3
PET (dual time point)	40	1	0
MR imaging	24	0	17

VEEG video electroencephalogram

An eight-channel head coil was used. The MRI sequences include T1-weighted 3D brain volumetric (BRAVO) imaging (gradient echo, flip angle 12°, TE/TR = 2.5/6.9 ms, section thickness 1 mm), axial-T2 with periodically rotated overlapping parallel lines with enhanced reconstruction (PROPELLER) (fast spin echo, TE/TR = 104/9000 ms, section thickness = 3 mm), axial-T2 fluid-attenuated inversion recovery (FLAIR) (fat-suppression fast spin echo, TE/TR = 104/9000 ms, time of inversion = 2475 ms, section thickness = 3 mm), diffusion-weighted imaging (DWI, b values = 0 and 1000 s/mm²), susceptibility-weighted imaging (SWI, gradient echo, flip angle = 15°, TE/TR = 4/45.5 ms, section thickness = 3.0 mm), and 3D arterial spin labeling perfusion-weighted imaging (3D ASL-PWI, post label delay = 1.5 s, section thickness = 4.0 mm).

Visual evaluation

The EZs on PET images at the same section acquired at both early and delayed time points were marked with arrows. The paired PET images were randomly assigned to two junior radiologists (Song Y and Song W). The two junior radiologists

have no knowledge of which image was acquired at early time point or delayed time point. They compared the difference of the labeled EZ with the contralateral region on PET images and selected the image with the most obvious difference, and then graded the selected images by using a 3-point scale: 0, no difference; 1, slight difference; 2, obvious difference.

Quantitative analysis of data

For SUV quantification and asymmetry index (AI) in brain cortical regions, an individual brain atlas registered with the ¹⁸F-FDG PET image was generated by statistical parametric mapping (SPM12, <http://www.fil.ion.ucl.ac.uk/spm/software/spm12>) based on 3D MR T1 images and automated anatomical labeling (AAL, <http://www.gin.cnrs.fr/en/tools/aal/>) atlas with 120 cortical regions. The data processing flow chart is shown in Fig. 1.

The 3D MR BRAVO T1 image data were segmented in SPM12 to generate white matter (WM), gray matter (GM), and cerebrospinal fluid (CSF) tissue probability maps (TPM). The deformation field image also obtained during the segmentation was used to nonlinearly deform the AAL atlas in Montreal Neurological Institute (MNI) template space to the data acquisition space where the atlas was registered with the PET/MRI. Then, the individual patient's GM in the MR images was defined in voxels with largest tissue probability in GM TPM and compared with WM and CSF TPMs and then was intersected with the deformed AAL atlas to obtain a final individual AAL atlas. To be applied in PET, the individual AAL atlas was down-sampled to match the resolution of the PET image and the SUV_{mean} in each cortical

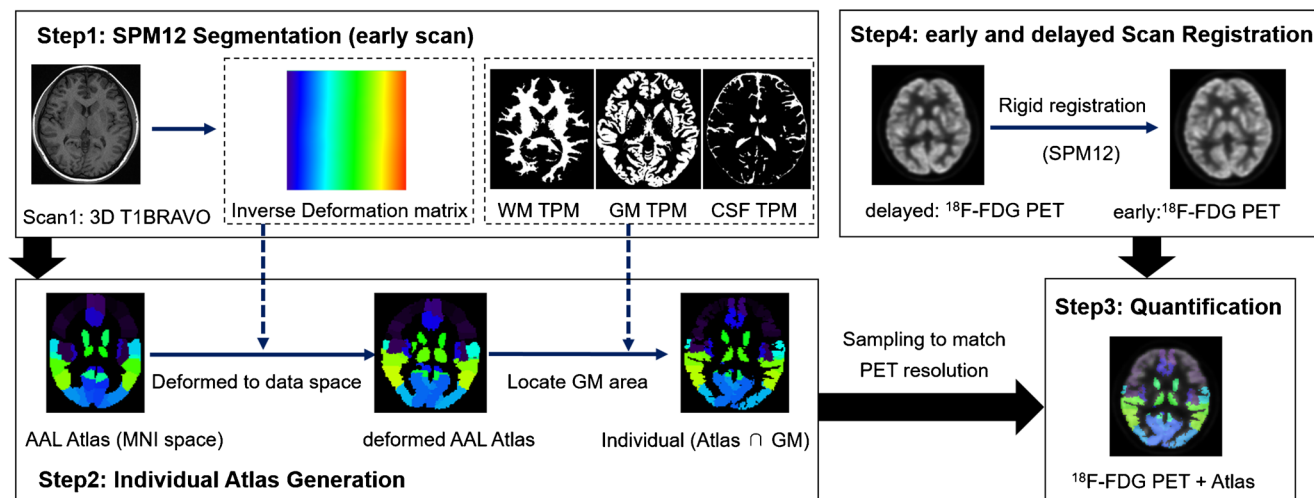


Fig. 1 Flow chart of data quantitative analysis. WM, white matter; GM, gray matter; CSF, cerebrospinal fluid; TPM, tissue probability map; AAL, automated anatomical labeling; MNI, Montreal Neurological Institute. Step 1: The 3D MR BRAVO T1 image data of early scan were segmented in SPM12 to generate inverse deformation matrix image and WM TPM, GM TPM, and CSF TPM. Step 2: The inverse deformation matrix image was used to nonlinearly deform the AAL atlas to generate deformed AAL atlas.

Then, the individual patient's GM TPM was intersected with the deformed AAL atlas to obtain a final individual AAL atlas. Step 3: The individual AAL atlas was down-sampled to match the PET resolution and the SUV_{mean} in each cortical region was extracted. Step 4: The delayed PET was rigidly co-registered with the early PET image and the SUV_{mean} was calculated with the same individual AAL atlas.

Table 3 AI variation between early and delayed time points in different groups

AI variation	MR imaging		Extra-TLE/TLE Extra-TLE (n = 31)	Delayed time point		
	MRI-positive (n = 24)	MRI-negative (n = 17)		TLE (n = 10)	Short delay (n = 32)	Long delay (n = 9)
AI2 > AI1	95.8% (23/24)	88.2% (15/17)	96.8% (30/31)	80.0% (8/10)	93.7% (30/32)	88.9% (8/9)
AI2 < AI1	4.2% (1/24)	11.8% (2/17)	3.2% (1/31)	20.0% (2/10)	6.3% (2/32)	11.1% (1/9)

AI1 AI at early time point, AI2 AI at delayed time point

region was extracted. For delayed imaging, the ¹⁸F-FDG PET was rigidly co-registered with the early PET image and the SUV_{mean} was calculated with the same individual AAL atlas.

The AI was calculated with SUV_{mean} in the EZ and the contralateral cortical regions using the following formula:

$$AI = 100 * 2 * (SUV_{mean_cont} - SUV_{mean_EZ}) / (SUV_{mean_cont} + SUV_{mean_EZ}) \tag{1}$$

The value of 100 added to the formula is to improve the scale for better data viewing.

The AI values at the early time points were marked as “AI1,” and the AI values at the delayed time points were marked as “AI2.” The difference in AI between the two time points was marked as ΔAI.

$$\Delta AI = AI2 - AI1 \tag{2}$$

Statistical analysis

Bland-Altman consistency analysis was applied to derive the AIs and a paired *t* test was used to compare the AIs for MRI-positive with MRI-negative, extra-TLE and TLE, and short delay and long delay. The kappa test was performed to evaluate the

consistency of visual assessment of the two observers. The Mann-Whitney *U* test was used to compare the scores of the two observers. A *P* value < 0.05 was considered statistically significant for the paired *t* test and the Mann-Whitney *U* test. For the kappa test, the kappa coefficient for the degree of agreement was defined as follows: poor agreement = < 0.20; fair agreement = 0.20–0.40; moderate agreement = 0.40–0.60; good agreement = 0.60–0.80; very good agreement = 0.80–1.00.

Results

SUV_{mean} AI results of dual time point ¹⁸F-FDG PET

Among the 41 cases, 38 (92.7%) cases had a larger AI at the delayed time than at the early time post-injection. The AI increased 95.8% in the MRI-positive patients, 96.8% in the extratemporal subjects, and 93.7% in the short delay subjects during the dual phase, which is higher than that in the MRI-negative, TLE, and long delay subjects (88.2%, 80.0%, and 88.9% respectively). There were only three cases with a decreased AI, including one case of MRI-positive with extra-TLE (hemorrhagic foci in the superior frontal gyrus) at short delay time, 1 case of MRI-negative with TLE at long delay time, and 1 case of MRI-negative with TLE at short delay time. The ΔAIs of these 3 cases were –1.94, –1.53, and –0.01, respectively (Table 3).

As shown in the results of the Bland-Altman analysis of AIs at dual time points (Fig. 2), the AIs of delayed time points were increased by a mean of 3.7 over the early time points, except for three beyond the limits of agreement.

The AIs were all significantly higher at the delayed time point in all groups. The ΔAIs were 3.71 ± 3.50 and 4.67 ± 7.94 for MRI-positive and MRI-negative; 4.52 ± 6.70 and 2.51 ± 2.42 for extra-TLE and TLE; and 4.24 ± 6.52 and 3.46 ± 2.90 for short delay and long delay groups, respectively. Among the groups, the highest AI1 and highest AI2 were found in the MRI-positive group. The lowest AI1 and lowest AI2 were found in the MRI-negative group. The MRI-negative group showed the highest ΔAI, while the temporal group showed the lowest ΔAI between the dual time points. The ΔAI of the short delay subjects (dual time points were

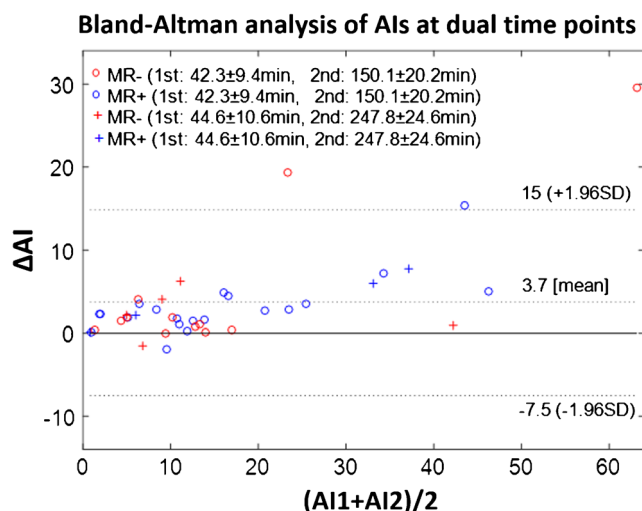


Fig. 2 Bland-Altman analysis of AIs at the early and delayed time points (MR+, MRI-positive; MR-, MRI-negative)

Table 4 AIs and Δ AI at early and delayed time points in different groups

Groups		AI1	AI2	Δ AI	P value
MR imaging	MRI-positive	17.76 \pm 11.26	21.47 \pm 13.92	3.71 \pm 3.50	0.0000
	MRI-negative	13.55 \pm 12.54	18.08 \pm 18.27	4.67 \pm 7.94	0.0009
Extra-TLE/TLE	Extra-TLE	15.31 \pm 12.08	19.98 \pm 16.95	4.52 \pm 6.70	0.0000
	TLE	17.40 \pm 11.82	19.91 \pm 13.61	2.51 \pm 2.42	0.0098
Delayed time	Short delay	15.55 \pm 11.30	19.80 \pm 16.30	4.24 \pm 6.52	0.0000
	Long delay	17.08 \pm 14.28	20.54 \pm 15.30	3.46 \pm 2.90	0.0098

AI1 AI at early time point, AI2 AI at delayed time point, Δ AI AI2-AI1

42.5 \pm 9.4 min and 150.1 \pm 20.2 min) was higher than that of the long delay subjects (dual time points were 44.6 \pm 10.6 min and 247.8 \pm 24.6 min) (Table 4).

The differences in SUV_{mean} between EZs and contralateral regions in the two time groups were compared (Fig. 3). Both the SUV_{mean} values of EZ (red circle) and the contralateral region (black circle) were increased at the delayed time point compared with those at the early time point at shorter and longer delays. But the SUV_{mean} increment in EZ side was less than that in the contralateral side.

Visual consistency analysis

The two observers, who had no knowledge of which images were early or delayed, compared the pairs of early time point and delayed time point images and selected the image with more obvious difference between the sides. Among the selected images from these two observers, 85.4% and 82.9%, respectively, were selected as the delay time point images. The kappa value between the two observers was 0.66 with good agreement. Based on the scores of all the images, there was no significant difference between the two observers. Figure 4

SUV_{mean} of EZ and contralateral region at dual time points

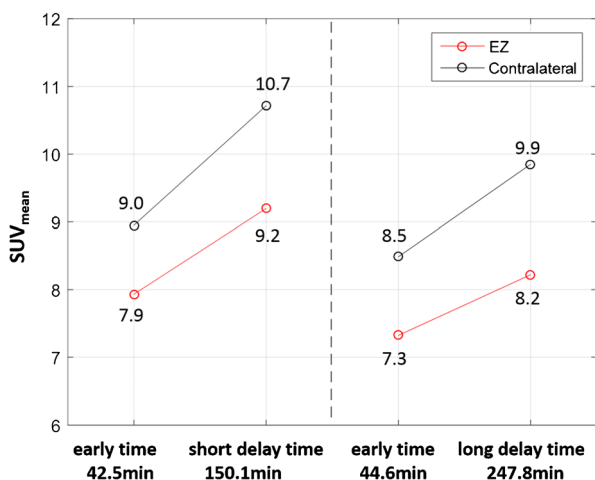


Fig. 3 SUV_{mean} variation of EZ and contralateral region at the short delay and long delay times

shows 4 different cases of EZ identification for dual time point PET images and MR images.

Discussion

In this study, we prospectively included 41 epileptic patients to acquire ^{18}F -FDG PET/MRI with early and one of two intervals of delayed imaging. By quantitative analysis of the differences in SUV_{mean} , AI, as well as visual evaluation of differences between early and delayed imaging, epileptic foci had more obvious relative hypometabolism compared with the contralateral regions on the delayed imaging than that on the early imaging. To the best of our knowledge, this is the first study to confirm that delayed PET/MRI could be used to better identify the EZ with relatively greater metabolic asymmetry between the EZ and contralateral regions.

Integrated PET/MRI is playing an increasingly important role in presurgical evaluation of EZ [14, 15]. PET/MRI can demonstrate pathologic findings by combining anatomic and metabolic abnormalities simultaneously acquired by MRI and PET. In this study, high-resolution MRI and functional MRI sequences, such as 3D BRAVO T1WI, T2WI, T2-FLAIR, SWI, and 3D ASL perfusion, offered accurate diagnostic information for subtle foci of encephalomalacia, small hemorrhagic foci, hippocampal sclerosis, arachnoid cysts, and brain malformations. These anatomic abnormalities corresponded with focal hypometabolism on PET. Some studies have shown good concordance between electroclinical data and the functional MR imaging data [16]. In addition, 3D ASL provides perfusion information and helps to confirm EZ localization. In another study, ^{18}F -FDG PET combined with 3D ASL increased the sensitivity and specificity for EZ to 100% and 90.9%, respectively [17]. Although in our study the localization of EZ was determined based on combining the clinical information, EEG, PET, and MRI findings by a consensus panel, and were not confirmed by surgical pathology, the results were still credible, and other studies have supported this approach [16, 18]. Without any ionizing radiation, MRI is the ideal anatomical imaging method for hybrid DTPI PET studies.

Based on currently accepted knowledge, hypometabolic brain foci are indicative of interictal EZs. Long-term recurrent

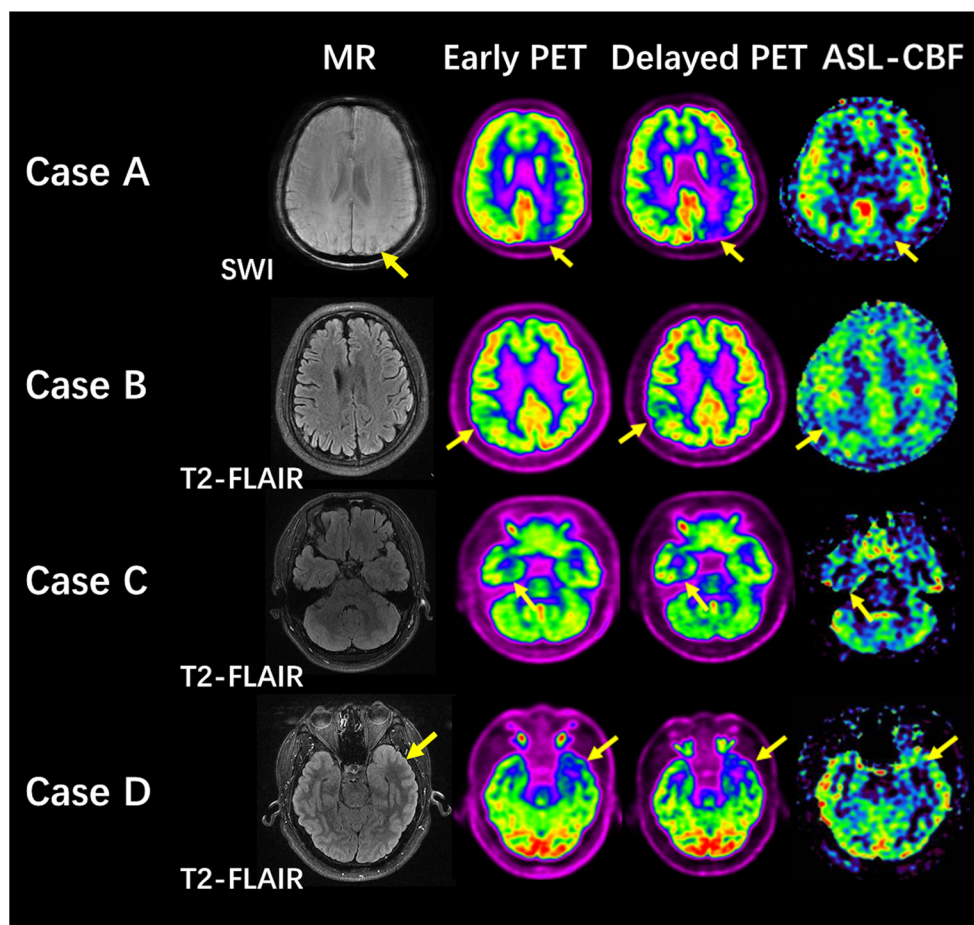


Fig. 4 EZ identification for dual time point PET images and MR images (EZs were marked with arrows). The EZs (arrows) were identified by comprehensive analysis of hypometabolic areas on dual time point PET, hypoperfusion on ASL-CBF, and MRI abnormalities. For all cases, focal hypometabolic areas were more severe at the delayed time point. Case A (patient no. 19): MRI-positive (small patches of hemorrhage in the left precuneus shown on SWI images) and extra-TLE at long delay time. The EZ was localized in the left precuneus. The AIs were 30.14 and 36.07 at the dual time point. Case B (patient no. 13): MRI-negative and extra-TLE at

long delay time. The EZ was localized in the right parietal lobe. The AIs were 5.01 and 10.20 at the dual time point. Case C (patient no. 26): MRI-negative and TLE at short delay time. The EZ was localized in the right temporal lobe. The AIs were 9.29 and 11.14 at the dual time point. Case D (patient no. 11): MRI-positive (swelling with hyperintensity in the left temporal lobe shown on T2-FLAIR images) and TLE at short delay time. The EZ was localized in the left temporal lobe. The AIs were 23.07 and 27.27 at the dual time point

seizures can cause additional morphological and functional abnormalities of neuron cells, including glucose transfer protein-1 dysfunction, neuron degeneration, neuronal loss, and decreased synaptic activity. These abnormalities lead to a lower ^{18}F -FDG uptake in the EZ compared with the contralateral region [3, 4, 17]. In this study, all the patients were interictal at the time of PET/MRI examination. The goal was to find the hypometabolic focus to localize the EZ. SUV_{mean} was used to quantify ^{18}F -FDG uptake in cortical regions, the AI was applied to quantify the differences between the EZ and contralateral regions, and ΔAI was applied to quantify the AI differences between early time and delay time points.

With prolonged time, both the EZ and the contralateral region had increased ^{18}F -FDG uptake at the delayed time point compared with that of the early time point, but the increased ^{18}F -FDG uptake in EZ was less than that in the

contralateral side due to the abnormalities of involved neuronal cells. As a result, at delay time, the AI of the EZ and the contralateral cortex increases. In this study, the AI was increased by a mean of 3.7 over that at the early time point. The difference between the EZ and the contralateral cortex glucose metabolism was more obvious at the delayed post-injection interval, making it easier to identify hypometabolic areas by visual evaluation. Among all groups in our study, the MRI-positive group showed the highest AI at both early and delayed time points. The hypometabolism in the lesions, especially in the encephalomalacia and hemorrhagic foci, can be easily identified at early time point. The MRI-negative group had the smallest AI at the early time point, but the biggest ΔAI between dual time points, suggesting metabolism asymmetry may be subtle at the early time point for MRI negative patients, but became obvious at the delayed time. However, it

should be pointed out that 2 out of 17 MRI-negative patients showed decreased AI at delay time; therefore, a further study with increased samples is needed.

Confirmed by EEG, MRI, and PET, 10–20% of temporal lobe epilepsy has shown hypometabolism in the contralateral region [3]. The possible mechanism could be that there are abnormal neural network activities in the cortex. The seizure discharge could be propagated by pathways of callosal fibers and fornix, suppressing the function of contralateral regions [3, 19]. The above reason will increase the difficulties of identifying the asymmetry in both hemispheres for cases with EZ in the temporal lobes by visual evaluation. In our study, minimal Δ AI was found in the TLE patients, with slightly further decreased AIs in two cases at the delay time. Although there were significant differences between the early and delayed AIs in TLE, the additive value of delayed time ^{18}F -FDG on TLE is not as high as that in extra-TLE.

The exact time of ^{18}F -FDG uptake plateauing in the cortex is still unclear, since ^{18}F -FDG uptake is still concentrating after 90 min [8, 20, 21]. For the published reports of DTPI PET for brain lesions, the delayed time of imaging after injection varies greatly from 30 min to 9.4 h [9, 22]. In our study, the early scan time was relatively fixed, about 40 min after injection, while the delayed scan time varied. Therefore, the cases were divided into two groups: a short delay time (mean 2.5 h) and a long delay time (mean 4 h). For both shorter and longer post-injection delay times, the AIs at the delayed time points were increased compared with the AIs at the early time point. But as the delay time extended, no greater Δ AI was found in the long delay cases than that in the short delay cases. In our study, the 2.5-h delay time seems better than the 4-h delay time, not only because of more noticeable asymmetry but also because it is more convenient for patients. A study of three-phase PET/CT body examination in differentiating between malignant and benign lesions also showed that a shorter delayed phase interval (110 min) was superior to a longer delayed phase interval (233 min) [13].

Although we proved that delayed ^{18}F -FDG hybrid TOF-PET/MRI is a feasible method to identify EZ, a few limitations existed in our study. First, we lacked surgery and histopathological confirmation as the gold standard. In our study, the EZ was identified by combined clinical history, EEG, PET, and multiple MRI sequences. But as mentioned before, the electro-clinical data has good concordance with functional MRI, and the combination of PET and MRI had high sensitivity and specificity for identifying the EZ [16, 17]. Second, all the patients were imaged at only two time points. A dynamic PET acquisition may help to show the course of glucose uptake by the EZ as well as to find an optimal delay time. Third, PET was not performed with a concomitant EEG. The concomitant monitorization with EEG is helpful to avoid a subclinical epileptic seizure which may cause reduced sensitivity in PET. Finally, in this study, to match the adult structure atlas better

and avoid the effects of sedative medicine on ^{18}F -FDG uptake, children under 12 years were excluded, in spite of the high incidence of epilepsy in children. Whether children are also suitable for delayed PET still needs further study.

Conclusions

Delayed ^{18}F -FDG PET/MRI can be used to better identify the epileptogenic zone with relatively greater metabolic asymmetry between the EZ and contralateral regions.

Acknowledgments We thank Libby Cone, MD, MA, from Liwen Bianji, Edanz Group China (www.liwenbianji.cn/ac), for editing drafts of this manuscript.

Funding information This work was supported by the Key Project of Hubei Province Technical Innovation (2017ACA182) and the Clinical Research Physician Program of Tongji Medical College, Huazhong University of Science and Technology (No. 5001530008).

Compliance with ethical standards

Conflict of interest The authors declare that they have no conflict of interest.

Informed consent All adult patients and the parents of pediatric patients gave written informed consent prior to enrollment in this study.

Research involving human participants and/or animals The research involved human participants. This prospective study was permitted by the Research Ethics Committee of the Huazhong University of Science and Technology.

References

1. Stanescu L, Ishak GE, Khanna PC, Biyyam DR, Shaw DW, Parisi MT. FDG PET of the brain in pediatric patients: imaging spectrum with MR imaging correlation. *Radiographics*. 2013;3(5):1279–303.
2. Lee SK. Surgical approaches in nonlesional neocortical epilepsy. *J Epilepsy Res*. 2011;1(2):47–51.
3. Kumar A, Chugani HT. The role of radionuclide imaging in epilepsy. Part 1. Sporadic temporal and extratemporal lobe epilepsy. *J Nucl Med*. 2013;54(10):1775–81.
4. Muhlhofer W, Tan Y-L, Mueller SG, Knowlton R. MRI-negative temporal lobe epilepsy—what do we know? *Epilepsia*. 2017;58(5):727–42.
5. Iwasaki M, Jin K, Nakasato N, Tominaga T. Non-invasive evaluation for epilepsy surgery. *Neurol Med Chir (Tokyo)*. 2016;56(10):632–40.
6. Zhu Y, Feng J, Wu S, Hou H, Ji J, Zhang K, et al. Glucose metabolic profile by visual assessment combined with statistical parametric mapping analysis in pediatric patients with epilepsy. *J Nucl Med*. 2017;58(8):1293–9.
7. Lamarche F, Job A-S, Deman P, Bhattacharjee M, Hoffmann D, Gallazzini-Crepin C, et al. Correlation of FDG-PET hypometabolism and SEEG epileptogenicity mapping in patients with drug-resistant focal epilepsy. *Epilepsia*. 2016;57(12):2045–55.

8. Spence AM, Muzi M, Mankoff DA, Finbarr O'Sullivan S, Link JM, Lewellen TK, et al. ^{18}F -FDG PET of gliomas at delayed intervals: improved distinction between tumor and normal gray matter. *J Nucl Med*. 2004;45(10):1653–9.
9. Kim D-W, Jung S-A, Kim C-G, Park S-A. The efficacy of dual time point F-18 FDG PET imaging for grading of brain tumors. *Clin Nucl Med*. 2010;35(6):400–3.
10. Mertens K, Acou M, Van den Broecke C, Nuyts R, Van Roost D, Achten E, et al. Progressive multifocal leukoencephalopathy (PML) mimicking high-grade glioma on delayed F-18 FDG PET imaging. *J Clin Neurosci*. 2012;19(8):1167–9.
11. Horky LL, Hsiao EM, Weiss SE, Drappatz J, Gerbaudo VH. Dual phase FDG-PET imaging of brain metastases provides superior assessment of recurrence versus post-treatment necrosis. *J Neuro-Oncol*. 2011;103(1):137–46.
12. Chan WL, Ramsay SC, Szeto ER, Freund J, Pohlen JM, Tarlinton LC, et al. Dual time point ^{18}F -FDG PET/CT imaging in the assessment of suspected malignancy. *J Med Imaging Radiat Oncol*. 2011;55(4):379–90.
13. Chen YM, Huang G, Sun XG, Liu JJ, Chen T, Shi YP, et al. Optimizing delayed scan time for FDG PET: comparison of the early and late delayed scan. *Nucl Med Commun*. 2008;29(5):425–30.
14. Ding Y-S, Chen B-B, Glielmi C, Friedman K, Devinsky O. A pilot study in epilepsy patients using simultaneous PET/MRI. *Am J Nucl Med Mol Imaging*. 2014;4(5):459–70.
15. Jadvar H, Colletti PM. Competitive advantage of PET/MRI. *Eur J Radiol*. 2014;83(1):84–94.
16. Galazzo IB, Mattoli MV, Pizzini FB, De Vita E, Barnes A, Duncan JS, et al. Cerebral metabolism and perfusion in MR-negative individuals with refractory focal epilepsy assessed by simultaneous acquisition of ^{18}F -FDG PET and arterial spin labeling. *Neuroimage Clin*. 2016;11:648–57.
17. Shang K, Wang J, Fan X, Cui B, Ma J, Yang H, et al. Clinical value of hybrid TOF-PET/MR imaging-based multiparametric imaging in localizing seizure focus in patients with MRI-negative temporal lobe epilepsy. *AJNR Am J Neuroradiol*. 2018;39(10):1791–8.
18. Morimoto E, Okada T, Kanagaki M, Yamamoto A, Fushimi Y, Matsumoto R, et al. Evaluation of focus laterality in temporal lobe epilepsy: a quantitative study comparing double inversion-recovery MR imaging at 3T with FDG-PET. *Epilepsia*. 2013;54(12):2174–83.
19. Jupp B, Williams J, Binns D, Hicks RJ, Cardamone L, Jones N, et al. Hypometabolism precedes limbic atrophy and spontaneous recurrent seizures in a rat model of TLE. *Epilepsia*. 2012;53(7):1233–44.
20. Villien M, Wey H-Y, Mandeville JB, Catana C, Polimeni JR, Sander CY, et al. Dynamic functional imaging of brain glucose utilization using fPET-FDG. *Neuroimage*. 2014;100:192–9.
21. Kimura N, Yamamoto Y, Kameyama R, Hatakeyama T, Kawai N, Nishiyama Y. Diagnostic value of kinetic analysis using dynamic ^{18}F -FDG-PET in patients with malignant primary brain tumor. *Nucl Med Commun*. 2009;30:602–9.
22. Prieto E, Martí-Climent JM, Domínguez-Prado I, Garrastachu P, Diez-Valle R, Tejada S, et al. Voxel-based analysis of dual-time-point ^{18}F -FDG PET images for brain tumor identification and delineation. *J Nucl Med*. 2011;52(6):865–72.

Publisher's note Springer Nature remains neutral with regard to jurisdictional claims in published maps and institutional affiliations.